

AUTHOR QUERY FORM

	<p>Journal: BMC</p> <p>Article Number: 9770</p>	<p>Please e-mail or fax your responses and any corrections to:</p> <p>E-mail: corrections.essd@elsevier.sps.co.in</p> <p>Fax: +31 2048 52799</p>
---	---	--

Dear Author,

Please check your proof carefully and mark all corrections at the appropriate place in the proof (e.g., by using on-screen annotation in the PDF file) or compile them in a separate list. Note: if you opt to annotate the file with software other than Adobe Reader then please also highlight the appropriate place in the PDF file. To ensure fast publication of your paper please return your corrections within 48 hours.

For correction or revision of any artwork, please consult <http://www.elsevier.com/artworkinstructions>.

Any queries or remarks that have arisen during the processing of your manuscript are listed below and highlighted by flags in the proof. Click on the 'Q' link to go to the location in the proof.

Location in article	Query / Remark: click on the Q link to go Please insert your reply or correction at the corresponding line in the proof
Q1	Please confirm that given names and surnames have been identified correctly.
Q2	Please check all affiliations, and correct if necessary.
Q3	Please check the telecommunication data for corresponding authors.
Q4	Please check the edit made in legend of Figure 3.

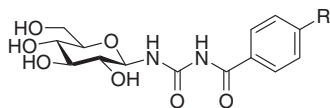
Thank you for your assistance.

Graphical abstract

***N*-(4-Substituted-benzoyl)-*N'*-(β -D-glucopyranosyl)ureas as inhibitors of glycogen phosphorylase: Synthesis and evaluation by kinetic, crystallographic, and molecular modelling methods**

pp xxx-xxx

Veronika Nagy, Nóra Felföldi, Bálint Kónya, Jean-Pierre Praly, Tibor Docsa, Pál Gergely, Evangelia D. Chrysina*, Costas Tiraidis, Magda N. Kosmopoulou, Kyra-Melinda Alexacou, Maria Konstantakaki, Demetres D. Leonidas, Spyros E. Zographos, Nikos G. Oikonomakos, Stanislav Kozmon, Igor Tvaroška, László Somsák*

R = Me, Ph, Cl, OH, OMe, NO₂, NH₂, COOH, COOMeBest inhibitor: R = Me $K_i = 2.3 \mu\text{M}$ 



Contents lists available at SciVerse ScienceDirect

Bioorganic & Medicinal Chemistry

journal homepage: www.elsevier.com/locate/bmc



N-(4-Substituted-benzoyl)-N'-(β-D-glucopyranosyl)ureas as inhibitors of glycogen phosphorylase: **Synthesis** and evaluation by kinetic, crystallographic, and molecular modelling methods [☆]

Q1 Veronika Nagy^{a,b}, Nóra Felföldi^a, Bálint Kónya^a, Jean-Pierre Praly^b, Tibor Docsa^c, Pál Gergely^d,
Evangelia D. Chrysiná^{e,*}, Costas Tiraidis^e, Magda N. Kosmopoulou^e, Kyra-Melinda Alexacou^e,
Maria Konstantakaki^e, Demetres D. Leonidas^{e,†}, Spyros E. Zographos^e, Nikos G. Oikonomakos^{e,‡},
Q2 Stanislav Kozmon^f, Igor Tvaroška^f, László Somsák^{a,*}

^a Department of Organic Chemistry, University of Debrecen, POB 20, H-4010 Debrecen, Hungary

^b Université Claude-Bernard Lyon 1, ICBMS, UMR UCBL-CNRS-INSA-CPE 5246, CPE-Lyon, 43 Boulevard du 11 Novembre 1918, F-69622 Villeurbanne, France

^c Cell Biology and Signaling Research Group of The Hungarian Academy of Sciences, University of Debrecen, Egyetem tér 1, H-4032 Debrecen, Hungary

^d Department of Medical Chemistry, Medical and Health Science Centre, University of Debrecen, Egyetem tér 1, H-4032 Debrecen, Hungary

^e Institute of Organic and Pharmaceutical Chemistry, The National Hellenic Research Foundation, 48, Vassileos Constantinou Avenue, GR-116 35 Athens, Greece

^f Institute of Chemistry, Slovak Academy of Sciences, Dubravska cesta 9, SK-845 38 Bratislava, Slovakia

ARTICLE INFO

Article history:

Received 5 October 2011
Revised 28 December 2011
Accepted 29 December 2011
Available online xxx

Keywords:

N-Acyl-N'-β-D-glucopyranosyl ureas
Glycogen phosphorylase
Inhibitor
X-ray crystallography
Molecular docking

ABSTRACT

N-(4-Substituted-benzoyl)-N'-β-D-glucopyranosyl ureas (substituents: Me, Ph, Cl, OH, OMe, NO₂, NH₂, COOH, and COOMe) were synthesised by ZnCl₂ catalysed acylation of O-peracetylated β-D-glucopyranosyl urea as well as in reactions of O-peracetylated or O-unprotected glucopyranosylamines and acyl-isocyanates. O-deprotections were carried out by base or acid catalysed transesterifications where necessary. Kinetic studies revealed that most of these compounds were low micromolar inhibitors of rabbit muscle glycogen phosphorylase b (RMGPb). The best inhibitor was the 4-methylbenzoyl compound (K_i = 2.3 μM). Crystallographic analyses of complexes of several of the compounds with RMGPb showed that the analogues exploited, together with water molecules, the available space at the β-pocket subsite and induced a more extended shift of the 280s loop compared to RMGPb in complex with the unsubstituted benzoyl urea. The results suggest the key role of the water molecules in ligand binding and structure-based ligand design. Molecular docking study of selected inhibitors was done to show the ability of the binding affinity prediction. The binding affinity of the highest scored docked poses was calculated and correlated with experimentally measured K_i values. Results show that correlation is high with the R-squared (R²) coefficient over 0.9.

© 2012 Elsevier Ltd. All rights reserved.

1. Introduction

Type 2 diabetes mellitus is currently estimated to affect more than 5% of the adult population in Western societies, and its incidence is expected to increase considerably in the future, in particular owing to the dramatic increase in obesity. The global incidence of type 2 diabetes is projected to afflict more than 300 million

people worldwide over the next 20 years, and many of those affected will be young adults.¹

The disease is characterised by hyperglycaemia associated with defective insulin production and hepatic and peripheral insulin resistance. Due to long term complications, it is a major cause of blindness and renal disease, and is known to significantly increase the risk of cardiovascular disorders.² Current preventive and therapeutic strategies do not achieve adequate control of blood glucose to prevent chronic morbidity, and are completely ineffective in ~40% of all diagnosed cases.³ As a consequence of this, there is a pressure on the research community (both academic and industrial) to develop novel healthcare interventions to address this substantial biomedical challenge.^{4,5}

Hepatic glucose output is elevated in type 2 diabetic patients and current evidence indicates that glycogenolysis (release of monomeric glucose from the glycogen polymer storage form) is

^{*} PDB ID Codes: 2QNB, 2QLM, 2QLN, 2QN3, 2QN7, 2QN8, 2QN9.

^{*} Corresponding authors. Tel.: +30 2107273851; fax: +30 2107273831 (E.D.C.); tel.: +36 52512900/22453; fax: +36 52453836 (L.S.).

E-mail addresses: echrysin@eie.gr, echry@tee.gr (E.D. Chrysiná), somsak@tigris.unideb.hu (L. Somsák).

[†] Present address: Department of Biochemistry and Biotechnology, University of Thessaly, 26 Ploutonos St., 41221 Larissa, Greece.

[‡] Dr. Nikos G. Oikonomakos sadly passed away on the 31st of August 2008 while this manuscript was in preparation. This paper is dedicated to his memory.

an important contributor to the abnormally high production of glucose by the liver.^{2,6,7} Glycogen phosphorylase (GP) is the enzyme responsible for glycogen breakdown to produce glucose and related metabolites for energy supply.^{4,8,9} Due to its key role in modulation of glycogen metabolism, pharmacological inhibition of GP has been regarded as an effective therapeutic approach to treating type 2 diabetes.^{10,11} Besides the liver tissue GP isoenzymes are also located in muscle and brain tissue with increased overall homology and high levels of identity at the catalytic site. Hence, series of studies have been underway, employing both the liver and the muscle isoenzyme for the design of new antidiabetic agents. Several classes of compounds have been reported and extensively surveyed^{3,10,12,13} for the inhibition of and in complex with liver and rabbit muscle GP (RMGP).

Distinct binding sites identified in GP¹⁴ include the catalytic site, the purine inhibitory site (also known as I-site), the allosteric site, the glycogen storage site, a novel allosteric inhibitor site and the newly discovered benzimidazole-binding site. The quest for compounds with higher potency than glucose to inhibit GP activity led to the design of various glucose-based analogues. For this purpose the properties of the catalytic site of GP in the *T* state (inactive) conformation were investigated. Specifically, the crystal structure of rabbit muscle enzyme revealed that the catalytic site is a long channel secluded from the bulk solvent. The entrance to this channel is constrained by a flexible loop (280s) comprising residues 282–286. During allosteric transition the 280s loop changes conformation and acts as a tollgate allowing access of the substrate to the core of the molecule. Dissection of the catalytic site in the presence of a collection of β -substituents of *p*-glucose unveiled two sub-sites of the catalytic channel, previously filled with water molecules in the native enzyme. These sites are lined by residues of mixed ionic/hydrophobic character.¹⁰ Glucose analogues, binding primarily to the catalytic site, represent the most populated family of GP inhibitors^{3,15} comprising among others various derivatives of *N*-acyl- β -D-glucopyranosylamines, glucopyranosylidene-spiro-heterocycles, *N*- and *C*- β -D-glucopyranosyl heterocycles as well as β -D-glucopyranosyl thiosemicarbazone derivatives.

A selection of *N*-acyl- β -D-glucopyranosylamine type compounds collected in Chart 1 indicate that increasing hydrophobicity of the acyl moiety makes the inhibition stronger (among **1** to **8**, **4** is the best inhibitor) while the α -D-anomer **9** is ineffective. Phosphorylated β -D-glucopyranosylamine **10** has a very weak effect. Spirocyclization with the proper 'anomeric' configuration (**11** and **12** vs **13**) makes very good inhibitors. Attachment of a further amide moiety to the first one (**14**, **15**) with a hydrophobic part results in inhibitor **15** whose efficiency is comparable to that of the spiro-hydantoin **11** and **12**. Crystallographic analyses of complexes of the above compounds with rabbit muscle glycogen phosphorylase *b* (RMGPb) demonstrated that in most cases a H-bridge exists between the β -D-glucopyranosylamine NH and main-chain carbonyl of His377 next to the active site (for illustration and references see Chart 1). This hydrogen bond in **1–4**, **6**, **7**, and **10–12** makes an important contribution to the binding. Consequently, α -D-configured derivatives **9** and **13** are much weaker inhibitors. This hydrogen bridge is absent in the complexes of compounds **5**, **8**, and **14** which again show poor binding. In the case of benzoyl urea **15** this H-bridge has not been observed in the crystal¹⁶ but the binding is stronger than in any other *N*-acyl- β -D-glucopyranosylamine derivative. This points to the role of interactions of the inhibitor molecule in the β -channel of the enzyme.

The aim of the present study is to investigate interactions of *N*-benzoyl-*N'*- β -D-glucopyranosyl urea derivatives in the β -channel. To this end **15** was modified by placing neutral apolar and polar, as well as acidic and basic substituents in position 4 of the phenyl ring. Experimentally determined and computed inhibition constants were compared to evaluate the predictive power of molecular

docking methods applied to the catalytic site of GP, while crystallographic studies of the enzyme-inhibitor complexes allowed to assess binding peculiarities of the molecules.

2. Results & discussion

2.1. Synthesis

Although there are many examples of *N*-substituted-*N'*-glycosyl urea derivatives in the literature, at the outset of this work we could find only two structures for *N*-acyl-*N'*-glycosyl ureas: per-*O*-acetylated *N*-acetyl- and *N*-benzoyl-*N'*-(β -D-glucopyranosyl)urea¹⁸ (per-*O*-acetyl protected **14** and **15**, respectively). These derivatives were made by exhaustive acetylation of β -D-glucopyranosyl urea by Ac₂O/ZnCl₂, and *N*-benzoylation of 2,3,4,6-tetra-*O*-acetyl- β -D-glucopyranosyl urea by BzCl/Py, respectively. For the synthesis of the planned new derivatives disconnections *A* and *B* (Scheme 1) were envisaged requiring investigation of reactions between β -D-glucopyranosylamines and acyl-isocyanates (*A*) and acylations of β -D-glucopyranosyl urea (*B*).

Intermediates for the preparation of the target compounds (Scheme 2) were obtained from 2,3,4,6-tetra-*O*-acetyl- β -D-glucopyranosyl azide (**17**). Per-*O*-acetylated β -D-glucopyranosylamine **18** was prepared by Raney-nickel reduction of **17**. The protected β -D-glucopyranosyl urea **16** was synthesized by a slight modification of a published protocol. *N*-Acylation of **16** with acid chlorides catalysed by ZnCl₂ in CHCl₃ gave compounds **20–24** in acceptable yields in most cases. For details of these transformations and referencing, please, consult Supplementary data.

The reaction of glucosylamine **18** with in situ prepared acyl-isocyanates¹⁹ was probed next. In these reactions the suggested solvent CH₃CN had to be dried with extreme care because even traces of moisture prevented the formation of the acyl-isocyanate. The yields of these transformations were also good except that for **23**. It can be concluded that for the preparation of the per-*O*-acetylated target compounds **19–24** *N*-acylation of urea **16** appears superior as compared to the other route taking into account the number and simplicity of the necessary manipulations.

Removal of the protecting groups was performed by the Zemplén method to get **15**, **27**, and **28**. These reactions had to be closely controlled by TLC in order to avoid loss of the *N*-acyl group after longer reaction times (cf. Scheme 2). This could not be achieved during Zemplén deprotection of **20**, **21**, and **24**, therefore, the respective **25**, **26**, and **29** were obtained by mild acid catalyzed transesterification. These problems associated with the deprotection were circumvented by elaborating a procedure to convert unprotected glucopyranosylammonium carbamate²⁰ (**35**) and acyl-isocyanates to *N*-acyl-*N'*- β -D-glucopyranosyl ureas, and for the preparation of **31–33** these conditions were used. Catalytic reduction of **29** furnished amino derivative **30**, while that of **33** gave carboxylic acid **34**.

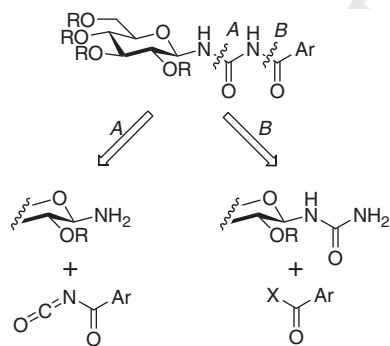
Structure elucidation of the new compounds was straightforward by NMR methods and needs no detailed comments (see Supplementary data for data). Carbonyl resonances of the acyl urea moieties appeared between 149–157 ppm (–NHCONH–) and 162–171 ppm (–NHCOAr).

2.2. Enzyme kinetics and X-ray crystallographic results

The inhibitory effect of ten new *N*- β -D-glucopyranosyl urea analogues **25–34** (Table 1) on the enzyme activity was evaluated by kinetic assays performed in the direction of glycogen synthesis at pH 6.8 and 30 °C. The results showed that all compounds are competitive inhibitors of the enzyme activity with *K*_i values in the low μ M range (Table 1). Among the substituents introduced in the *para*-position of the phenyl ring only the –CH₃ (compound **25**) appeared

N–H···O=C				K_i [μM]									
H-bridge													
+	1	R = CH ₃		32	<p>H-bridges between His-377 and <i>N</i>-acyl-β-D-glucopyranosylamine type inhibitors in the catalytic site of GP</p>								
+	2	R = CF ₃		75									
+	3	R = C ₆ H ₅		81									
+	4	R = C ₁₀ H ₇											
		(2-naphthyl)		10									
-	5	R = NH ₂		140									
+	6	R = CH ₂ N ₃		49									
+	7	R = CH ₂ CH ₂ CO ₂ H		20									
-	8	R = COOCH ₃		210									
-	9		non inhibitory										
+	10			5900									
+	11	X = O		3.1									
+	12	X = S		5.1									
				29									
-	13			320									
				105									
					<table border="1"> <thead> <tr> <th>N–H···O=C</th> <th>K_i [μM]</th> </tr> </thead> <tbody> <tr> <td>H-bridge</td> <td></td> </tr> <tr> <td>-</td> <td>14 370</td> </tr> <tr> <td>-</td> <td>15 4.6</td> </tr> </tbody> </table>	N–H···O=C	K_i [μM]	H-bridge		-	14 370	-	15 4.6
N–H···O=C	K_i [μM]												
H-bridge													
-	14 370												
-	15 4.6												

Chart 1. Selected *N*-acyl- β -D-glucopyranosylamine type inhibitors of GP.^{15,17}



Scheme 1. Retrosynthetic disconnections of *N*-acyl-*N'*-(β -D-glucopyranosyl) urea.

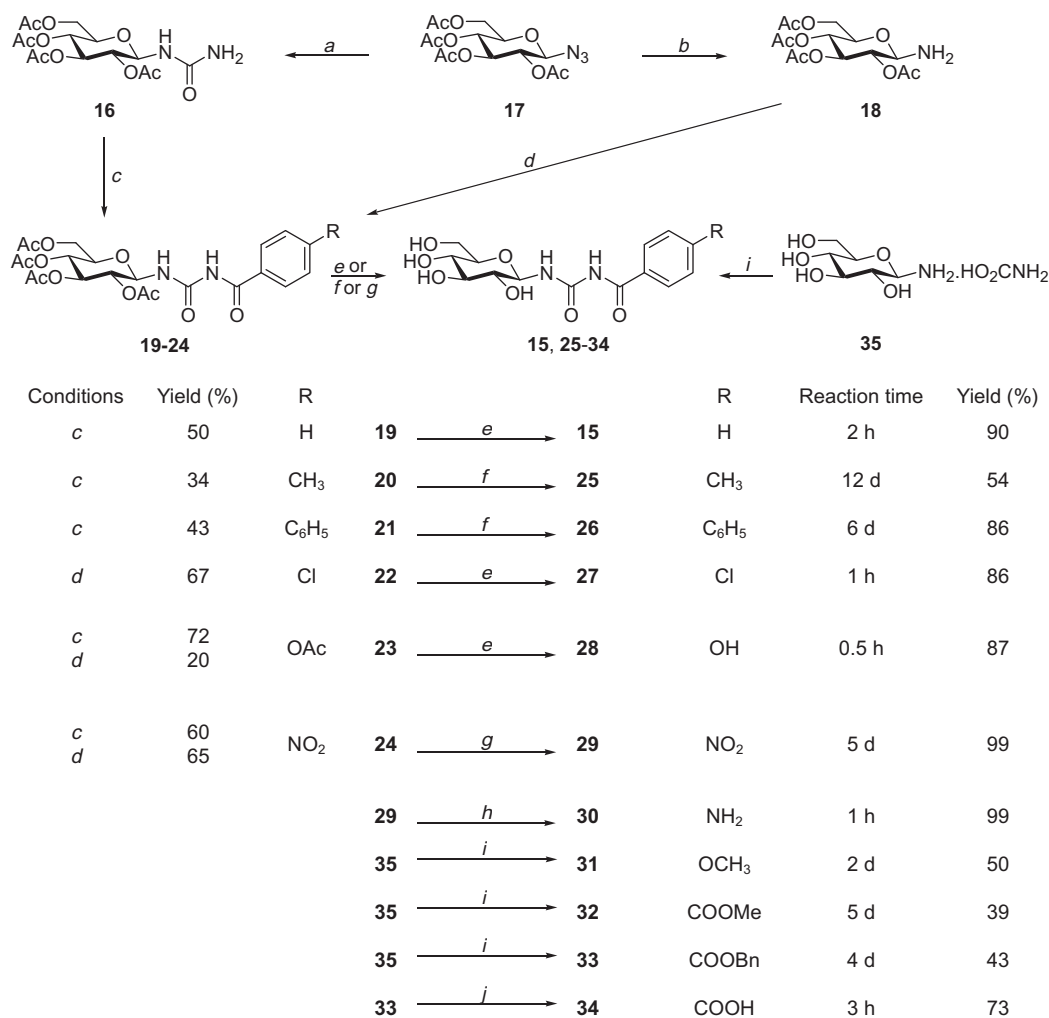
to bring about slightly improved affinity (K_i value of 2.3 μM) compared to the lead compound **15**.

With the aim to interpret the results obtained from the kinetic experiments and provide rationalizations of the binding affinities, structural studies of RMGPb in complex with six new compounds **25–30** were performed at high resolution (Table 1). All derivatives of **15** bound at the catalytic site, as it was clearly indicated by the $2F_o - F_c$ and $F_o - F_c$ electron density maps (Fig. 1a–f). Additional

electron density was observed at the new allosteric site for compound **29** (Fig. 1g), suggesting weak binding. All six inhibitors induced extended conformational changes mainly in the 280s loop upon binding, similar, not identical though, to those observed in the RMGPb:**15** complex.¹⁶ More detailed analysis of the complex structures was performed by mapping the key hydrogen bond and van der Waals interactions formed with residues lining the catalytic site (Tables S2b and S2c). The interactions formed by the peripheral hydroxyl groups of the glucopyranose moiety at the catalytic site are maintained in almost all complexes. Therefore, the analyses focused on the alterations in the network of contacts that occur when a new neutral, apolar and polar or slightly acidic and basic functional group was introduced to the parent molecule (at position 4 of the phenyl ring).

2.2.1. Compound 15

The crystal structure of RMGPb–**15** complex (Bzurea) was previously determined to 1.8 Å resolution¹⁶; the structural results showed that upon binding of **15** at the catalytic site, there is a significant rearrangement of the 280s loop. In specific, Asn284 is sandwiched between the side chains of residues Phe285 and Tyr613, resulting in the disruption of the inhibitor site located at the entrance of the catalytic channel. The dramatic shift observed in the 280s loop (shifts ~ 1.3 to 3.7 Å of C α atoms compared to



Scheme 2. Reagents and conditions: (a) PPh₃, EtOAc, NH₃, CO₂, rt, 88%; (b) H₂, Raney-Ni, EtOAc, rt, 71%; (c) 4-R-C₆H₄-COCl, ZnCl₂, CHCl₃, reflux; (d) 4-R-C₆H₄-CONCO, CH₃CN, Ar, rt; (e) NaOMe, MeOH, rt; (f) AcCl, MeOH, rt; (g) KHSO₄, MeOH, rt; (h) H₂, Raney-Ni, MeOH, rt; (i) 4-R-C₆H₄-CONH₂ converted to 4-R-C₆H₄-CONCO (by (COCl)₂ in ClCH₂CH₂Cl at reflux temp., then reaction with **35** in Py, rt; (j) H₂, Pd/C, MeOH, reflux.

the native structure) was attributed to the bulky benzoyl moiety; however, these shifts were not in the direction of *T* to *R* allosteric conversion. The conformational changes resulted in increased contacts between the inhibitor and the protein, providing a rationalization for the *K_i* with a value of 4.6 μM. However, the ‘characteristic’ hydrogen bond between amide nitrogen N1 and the backbone O of His377 was disrupted in RMGPb-**15** complex.¹⁶ This hydrogen bond was present in most RMGPb structures determined in complex with β-D-glucopyranosylamine analogues illustrated in Chart 1.

2.2.2. Compound 25

Introduction of a methyl (-CH₃) group in the *para*-position of the phenyl ring resulted in an improved inhibitor with a *K_i* value of 2.3 μM compared to the lead compound **15**. Structural studies of RMGPb-**25** complex showed that **25** bound at the catalytic site and formed a total of 18 hydrogen bonds and 94 van der Waals interactions (slightly reduced compared to **15**, **20** and **103**, respectively) (Tables S2b and S2c and Fig. 2a and b). The aforementioned ‘characteristic’ hydrogen bond between N1 and the main chain O of His377 was disrupted in accordance with the results observed for Bzurea. The substituted phenyl ring pointed at a similar direction to that of **15** with a negligible incline (atoms shifted by ~0.4 to 0.7 Å) towards Ala383 (Fig. 3a). The solvent structure was comparable in

both complex structures except for two water molecules, Wat161 O and Wat235 O (numbering from RMGPb:**15** complex structure) that were displaced to avoid clashes with C15 of the methyl group. A few minor shifts were also recorded in the solvent lying in the vicinity of the hydrophobic -CH₃ group, that is Wat84 O shifts by ~0.7 Å, Wat215 O by ~0.6 Å and Wat209 O by ~0.5 Å (Wat93 O, Wat251 O, Wat183 O numbering from RMGPb-**15** complex, respectively). The rearrangement of the solvent structure induces more profound changes in the 280s loop compared to those observed in the Bzurea complex. In particular, the side chain of Asn282 became less stable mainly due to the displacement of Wat235 O in the presence of the -CH₃ group and changed conformation by rotation of its dihedrals (χ₁, χ₂) by (~120°, 33°), respectively. As a result the side chain of Asn284 is subjected to a minor shift in all atoms by ~0.5 Å. Similar move (by ~0.5 Å in all atoms) was recorded for Phe285 since the hydrogen bond formed between the backbone oxygen and Asn282 ND2 was disrupted. Analogous changes were induced to the side-chain atoms of Phe286 (atoms shifted by 0.5 to 0.7 Å and ψ rotated by ~10°). However, the most profound modifications, possibly interrelated to the new position of Asn282, were observed in Glu287 that adopted a different conformation (rotation of dihedral angles (χ₁, χ₂, χ₃) by (~55°, ~18°, ~170°), respectively) compared to RMGPb:**15** complex structure. The peptide bond between Glu287 and Gly288 also flipped to restore stereochemistry.

Table 1
Kinetic data obtained with rabbit muscle GPb and crystallographic numbering of the compounds

Compound	R	K_i (μM)	Compound	R	K_i (μM)
15		4.6 ± 0.90^{16}	30		6.0 ± 0.60
25		2.3 ± 0.03^a	31		3.2 ± 0.16
26		3.7 ± 0.06	32		4.0 ± 0.16
27		4.4 ± 0.09^a	33		150 ± 12^a
28		6.3 ± 0.30	34		85 ± 6.5^a
29		3.3 ± 0.30			

^a K_i values for these compounds were calculated for comparison purposes by the Cheng–Prusoff equation: $K_i = IC_{50}/(1 + [S]/K_m)$.

Although binding of **25** seemed to provoke more profound changes in the 280s loop than those of **15**, and some perturbation in the solvent structure, introduction of $-\text{CH}_3$ appeared to be overall energetically favourable since it outweighed those changes and resulted in a better inhibitor than **15**.

2.2.3. Compound 26

Replacement of the methyl group by another hydrophobic but much bulkier substituent ($-\text{C}_6\text{H}_5$) in the *para*-position of the phenyl ring was also investigated. The new compound exhibited similar affinity to **25** (K_i value of $3.4 \mu\text{M}$) and bound at the catalytic site with the phenyl ring been subjected to minor incline (atoms shifted by ~ 0.3 to 0.5 \AA) compared to the corresponding one in **15** complex (Fig. 3b) towards Asn133 and Glu88 (unlike RMGPb:**25** that moves slightly towards Ala383). The new aromatic ring introduced was rotated by $\sim 38^\circ$ to optimize its interactions with residues in the vicinity Asn282, Phe286, Arg292, and His341. The ($-\text{C}_6\text{H}_5$) group occupied the subsite of the β -pocket at the catalytic channel²¹ displacing three water molecules Wat84 O, Wat161 O and Wat215 O upon binding to avoid clashes with C17 atom of the second phenyl ring. These two waters were hydrogen bonded to Wat235 O, also absent in the new complex structure that was in turn interacting with Asn282 ND2. Disruption of this water-mediated network destabilized the side chain of Asn282 that adopted a different conformation by rotation of its dihedrals (χ_1 , χ_2) by ($\sim 130^\circ$, $\sim 35^\circ$) similar to that in RMGPb:**25**. The

alteration of Asn282 side chain resulted in shifts in the range of ~ 0.3 to 0.7 \AA in both Asn284 and Phe285 side chain atoms and more pronounced modifications in Glu287. The peptide bond formed between Glu287 and Gly288 flipped as in RMGPb:**26** complex and the side chain of the former also changed (rotation of dihedral angle χ_3 by $\sim 61^\circ$). Introduction of such a bulky substituent affects also the side chain of Arg292 the atoms of which are slightly shifted away from the ligand (by $\sim 0.5 \text{ \AA}$). Overall, **26** upon binding maintains the number of hydrogen bond interactions formed compared with the methyl compound **25**; however, the increased number of van der Waals interactions (113) did not seem to promote ligand binding (Fig. 2c, Tables S2b and S2c). The preference though of the β -pocket subsite for more hydrophobic and the space availability for even bulkier substituents became evident.

2.2.4. Compound 27

To further investigate the type of interactions formed at the catalytic site a chlorine atom ($-\text{Cl}$) was placed in position 4 of the phenyl ring. Kinetic results indicated that affinity of the new analogue was equivalent to that of the parent molecule (K_i value of $4.4 \mu\text{M}$). Analysis of the RMGPb:**27** crystal structure showed that it bound at the catalytic site in a similar fashion to the previous analogues (Fig. 3c) making a total of 19 hydrogen bond and 91 Van der Waals interactions (Fig. 2d, Tables S2b and S2c). The phenyl ring was

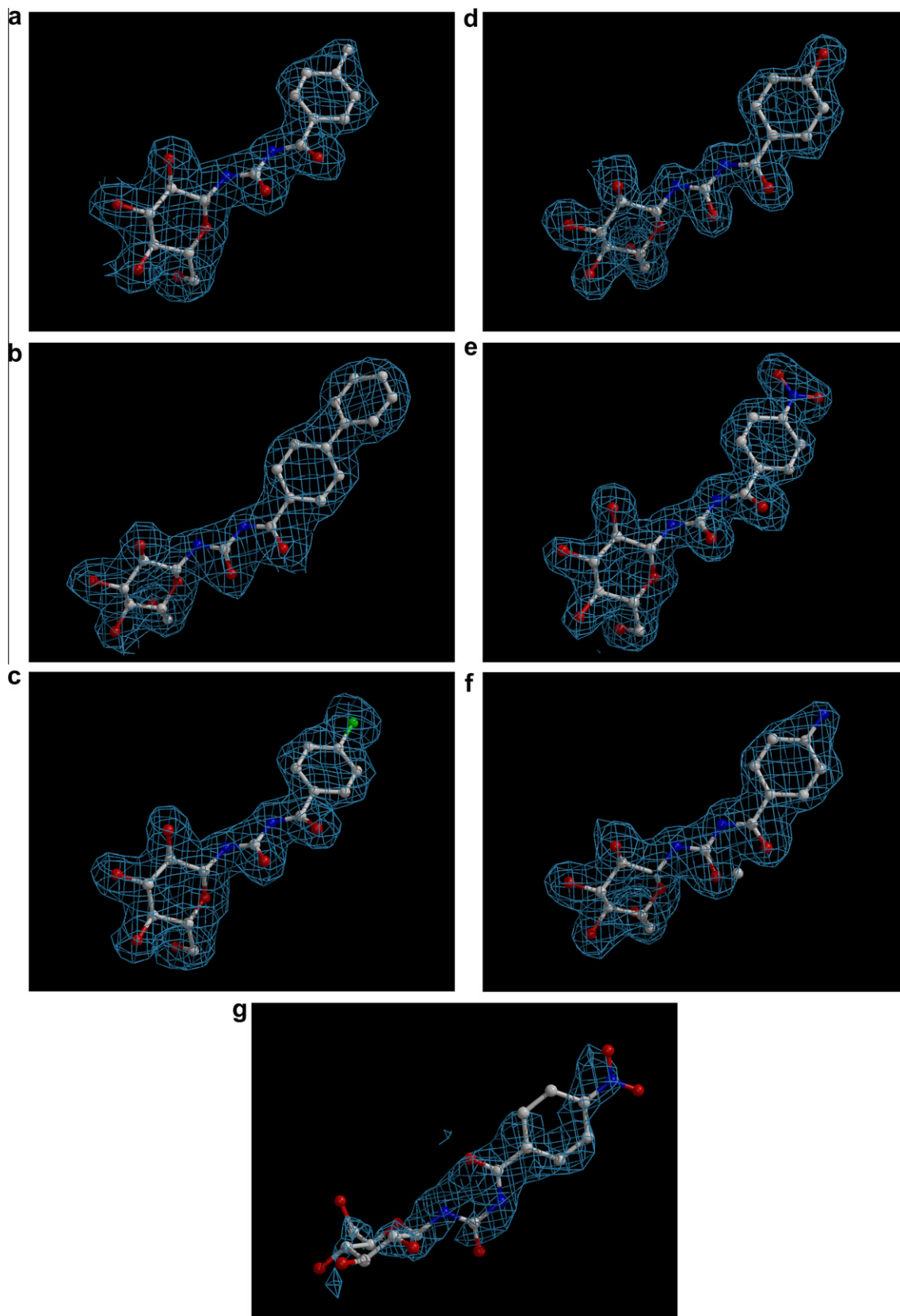


Figure 1. Schematic representation of the $2F_o - F_c$ electron density maps contoured at 1.0σ level of the refined Bzurea analogues bound at the catalytic site of RMGPb (a, b, c, d, e, f for compounds **25**, **26**, **27**, **28**, **29**, **30**) and the new allosteric site (g, compound **29**).

almost coplanar with the one in **15**, and only slight shift (by ~ 0.3 to 0.5 \AA) of the carbon atoms towards Ala383 was observed compared

to **15** when bound to RMGPb (Fig. 3c). Two water molecules are displaced upon binding of **27** at the catalytic site; Wat161 O to

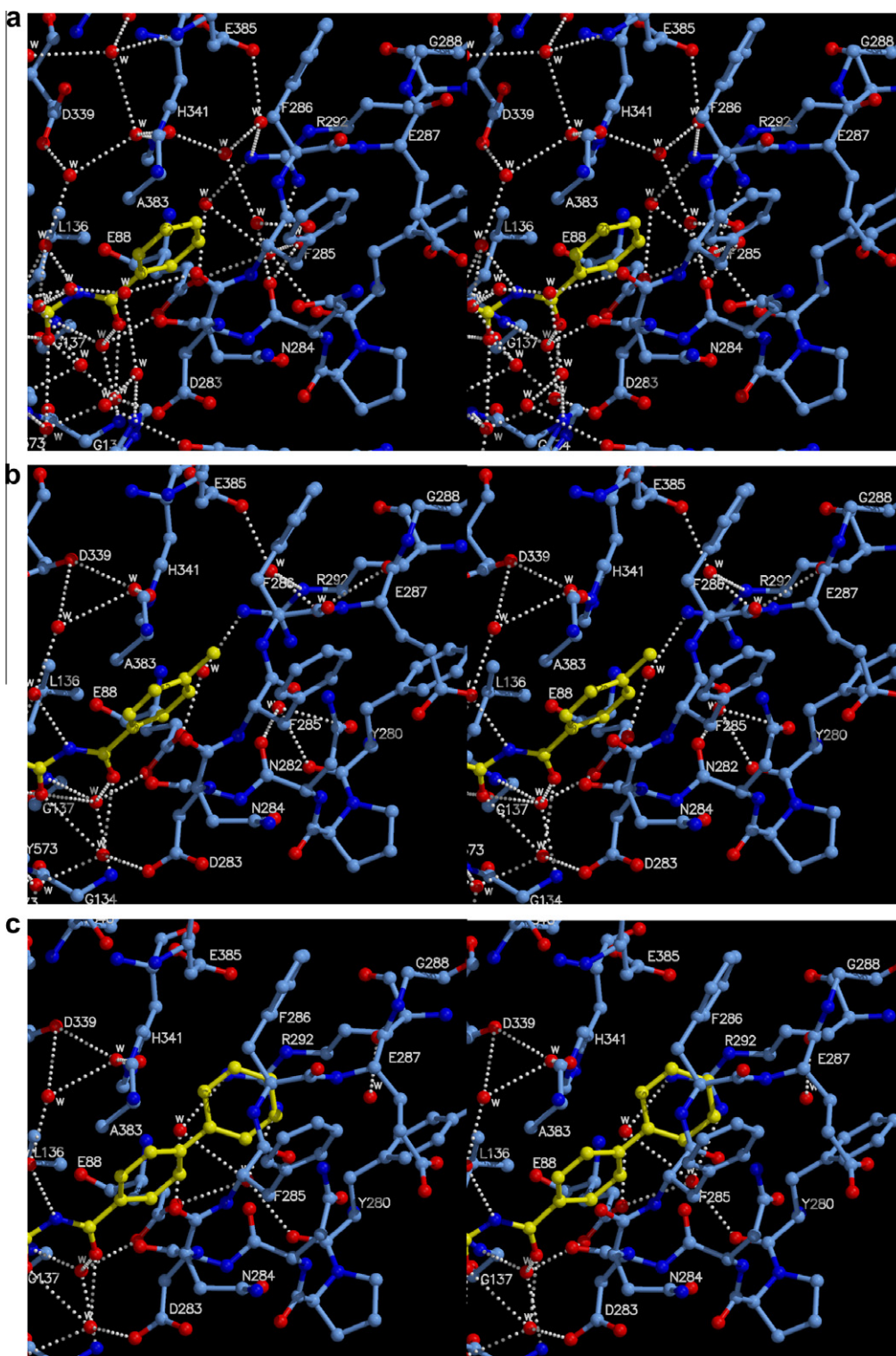


Figure 2. Stereo representation of the molecular interactions of compounds **15** (a), **25** (b) **26** (c), **27** (d), **28** (e), **29** (f), **30** (g) when bound at the catalytic site of RMGPb and protein atoms in the vicinity. Water molecules are labeled as w. Emphasis is given in the new substituent introduced in the *para*-position of the phenyl ring of **15**.

330

avoid clashes with the chlorine atom and its neighboring Wat235 O that was not tightly bound at the catalytic site any more also due to the conformational change of Asn282 side chain (dihedral angles χ_1 , χ_2 rotate by $\sim 120^\circ$, $\sim 40^\circ$, respectively) that resulted in the disruption of the second hydrogen bond interaction it formed with ND2 atom of the same residue. Additional alterations observed in the solvent structure involved shifts of Wat215 O (Wat257 O numbering from GPb:**25** complex), Wat84 O (Wat87

O), Wat236 O (Wat186 O), Wat148 O (Wat270 O) by ~ 0.8 , ~ 0.7 , ~ 0.3 , ~ 0.9 Å, respectively. Overall, residues of the 280s loop follow the same rearrangement observed for in the RMGPb:**15** crystal structure except for Asn282. Upon ligand binding, residues Asn284, Phe285, Phe286 are subjected to minor disturbance (in the range of ~ 0.3 to 0.7 Å). More extensive changes are recorded for Glu287 the peptide bond of which with Gly288 flipped in this complex structure as well. Despite the increased perturbation of

340

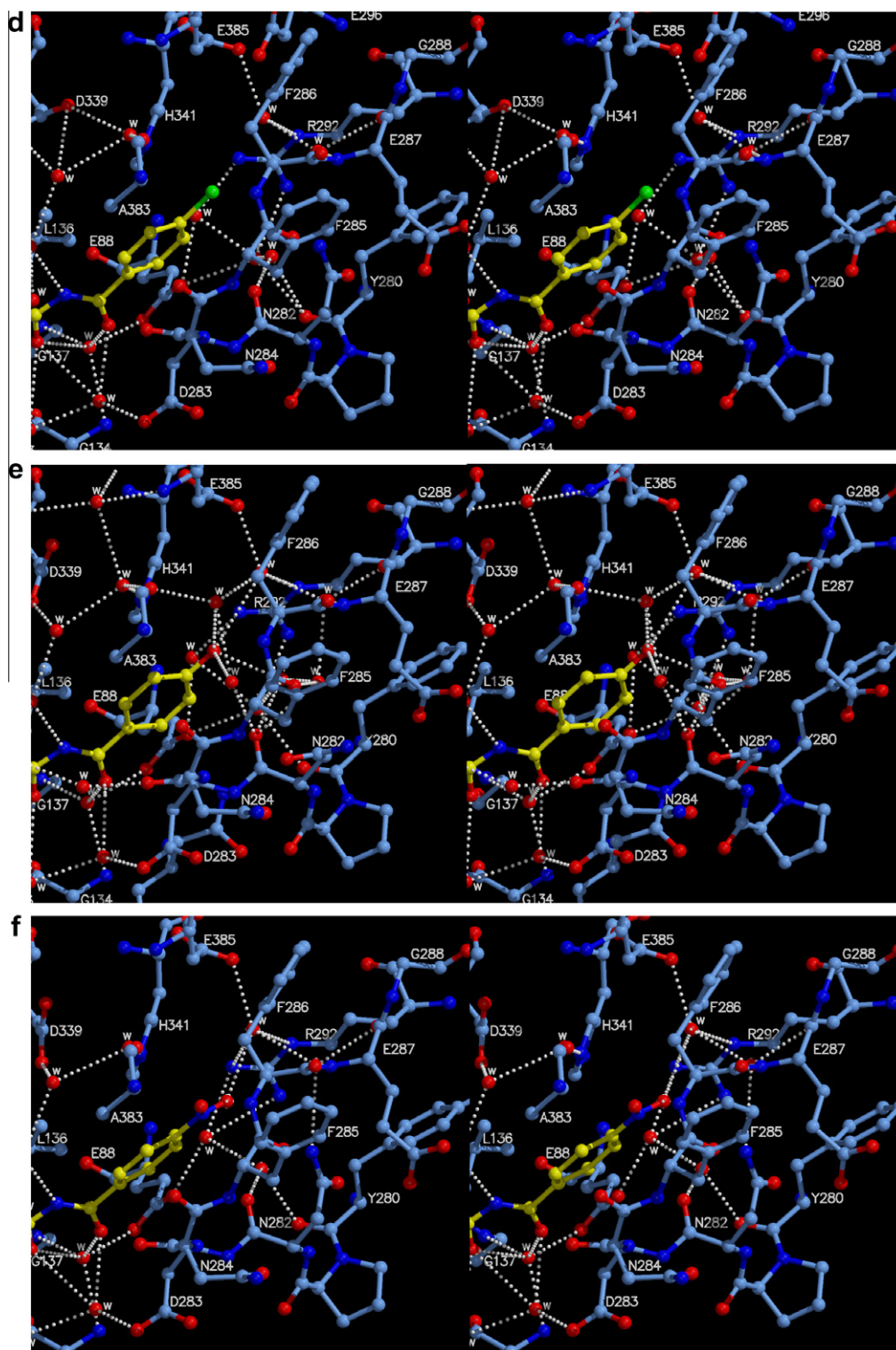


Fig. 2 (continued)

the 280s loop residues it appeared that the addition of chlorine atom and the amendments of the solvent structure at the catalytic subsite outweighed the energy loss and resulted in an inhibitor as potent as the lead compound.

2.2.5. Compound 28

Replacement of the chlorine atom by -OH in the *para*-position of the phenyl ring appeared to be less favourable as indicated by

the kinetic evaluation (K_i increased to a value of 6.3 μM). Compound **28** bound at the catalytic site of RMGPb with the phenyl ring atoms lying in approximately the same position as in Bzurea (atoms shift by ~ 0.3 Å) (Fig. 3d). It induced similar conformational changes in the 280s loop residues to the ones observed previously in Bzurea complex, but less extended than those in the complex structures of compounds **25**, **26** and **27**. Most of the residues lining the 280s loop including Asn282 were subjected only to subtle

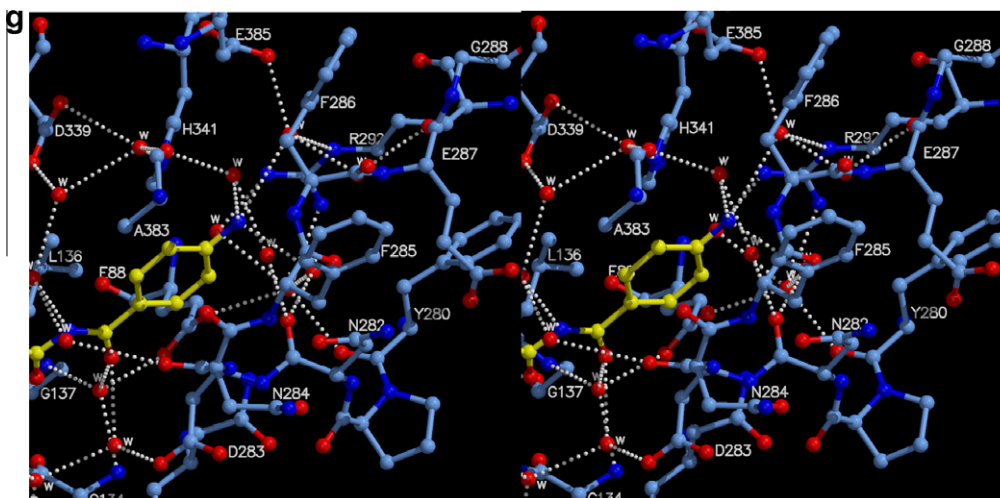


Fig. 2 (continued)

changes (atoms shifted by ~ 0.3 to 0.5 Å in Asn282, Asn284, Phe285, Phe286) and the most profound difference is that observed in the flipping of the peptide bond between Glu287 and Gly288 in accordance with the aforementioned 4-substituted Bzurea analogues. In general, the ligand's contacts with protein and water residues in the vicinity of the catalytic site were almost maintained compared to RMGPb:**15** structure (22 hydrogen bonds, 104 van der Walls interactions) (Fig. 2e). Focusing on the $-OH$ group (atom O12 of **28**) the complex structure showed that it was implicated in potential water-mediated interactions with the side chain atoms of residues Glu88, Arg292, Glu385 and the backbone oxygen atoms of Tyr280, Asn282 and Ala383 through water molecules Wat86 O, Wat166 O, Wat224 O, Wat244 O and Wat333 O. Little rearrangement was also observed in the solvent structure in the environment ranging from ~ 0.3 to 0.8 Å involving mainly water molecules Wat84 O, Wat161 O, Wat215 O, Wat235 O). Apparently, the results indicated by RMGPb:**28** complex structure indicated that $-OH$ was not advantageous, although it induced less modifications upon binding compared to the rest of the analogues studied.

2.2.6. Compound 29

Substitution of $-OH$ group by a $-NO_2$ group resulted in a slightly more potent inhibitor with a K_i of 3.3 μM . Structural results derived from RMGPb:**29** complex showed that binding of the new analogue caused an incline of the phenyl ring by $\sim 10^\circ$ compared to Bzurea and shifts of the corresponding carbon atoms in the range of ~ 0.4 and ~ 0.8 Å (Fig. 3e). Binding of **29** was stabilized by an extended network of hydrogen bond interactions with the catalytic site residues, mainly through water molecules. The total number of hydrogen bonds was increased to 23 as compared to 20 in the case of Bzurea and van der Waals interactions were maintained to 103 (Fig. 2f, Tables S2b and S2c). Two water molecules, Wat161 O and Wat235 O (numbering from RMGPb:**15**) were displaced upon ligand binding to avoid clashes with O10 of the $-NO_2$ group. The ligand oxygen O9 is hydrogen bonded to Arg292 NE, NH2 and Glu385 OE2 (through Wat86 O) to Asn282 ND2 and Glu287 N, O (through waters Wat315, Wat316), to Tyr280 O, Asn282 O (through waters Wat316 and Wat224) and Glu88 OE1 and Arg292 NH1, NH2 (through waters Wat316, Wat224 and Wat218) (Fig. 2f, Table S2b). In addition, the solvent network got slightly distorted particularly at the β -pocket where the positions of water molecules changed to optimize the interactions upon binding of **29**. In specific, waters Wat224 O, Wat86 O, Wat245 O, Wat218 O shifted by ~ 1.0 , ~ 0.6 , ~ 0.4 , ~ 1.1 Å, respectively, inducing displacement of Wat231 O that is missing in the new complex structure. Minor rearrangement of

the solvent structure appeared in the rest of the catalytic channel with shifts in the range of ~ 0.4 to ~ 0.9 Å. The side chain of Asn282 adopts an alternate conformation (torsion angles χ_1 , χ_2 rotate by $\sim 131^\circ$ and $\sim 36^\circ$, respectively) similar to the one observed in the rest of the Bzurea analogues studied except $-OH$. Further changes recorded in the 280s loop residues involve the side chain atoms of Asn284 (shifted by ~ 0.3 to 0.5 Å), Phe285 (rotation of dihedral χ_2 by $\sim 15^\circ$ and Ca shifted by ~ 0.5 Å), Phe286 (all atoms shifted by ~ 0.5 to ~ 0.8 Å) and Glu287 (rotation of dihedrals, χ_1 , χ_2 , χ_3 by $\sim 18^\circ$, 20° , 131° , respectively and atoms shifted by ~ 0.7 to ~ 1.6 Å). The backbone atoms of Glu287 occupied a new position at ~ 0.3 to 0.5 Å away from the one in RMGPb:**15** promoting the change of the peptide bond with Gly288 by 180° . Despite the extended changes that binding of **29** induces at the catalytic site of the enzyme mainly in the 280s loop residues Asn282 and Glu287 along with the rearrangement of the solvent structure to accommodate the $-NO_2$ group, the results indicated that binding of **29** is favourable stabilizing the 280s loop in the closed conformation a little better compared to the lead compound Bzurea.

2.2.7. Compound 30

Further modification involved introduction of a $-NH_2$ group in the *para*-position of the phenyl ring that resulted in a less potent inhibitor compared with **15** with a K_i value of 6.0 μM . The structural data from the RMGPb:**30** complex showed that the phenyl ring inclined slightly ($\sim 12^\circ$) when the new substituent was introduced and the carbon atom C12 showed a minor shift (less than 0.5 Å) (Fig. 3f). The network of interactions formed by **30** upon binding was very similar to that of Bzurea (21 hydrogen bonds, 98 van der Waals contacts) (Fig. 2g). N3 Atom of the $-NH_2$ group did not form any direct hydrogen bonds with residues lining the catalytic site, however, it was involved in water mediated contacts with the 280s and 380s loop residues as well as Arg292, through water molecules Wat86, Wat166 and Wat224 (Fig. 2g). The 280s loop adopts the same orientation as in the RMGPb:**15** complex structure with minor conformational changes. The position of Asn284 side chain atoms changed by ~ 0.3 to 0.4 Å and similar shifts were recorded for the main chain atoms of Phe285 while its dihedral angle χ_2 rotated by $\sim 18^\circ$. The backbone atoms of Phe286 also shifted by ~ 0.3 to 0.5 Å and the most significant change was in the peptide bond between Glu287 and Gly288 that flipped also in this complex structure compared to RMGPb:**15**. Only minor changes were observed in the water structure at the catalytic site upon binding of **30** to facilitate the interactions formed by N3 of the amino group introduced with the environment. These involve shifts of Wat250 O (by ~ 1.2 Å),

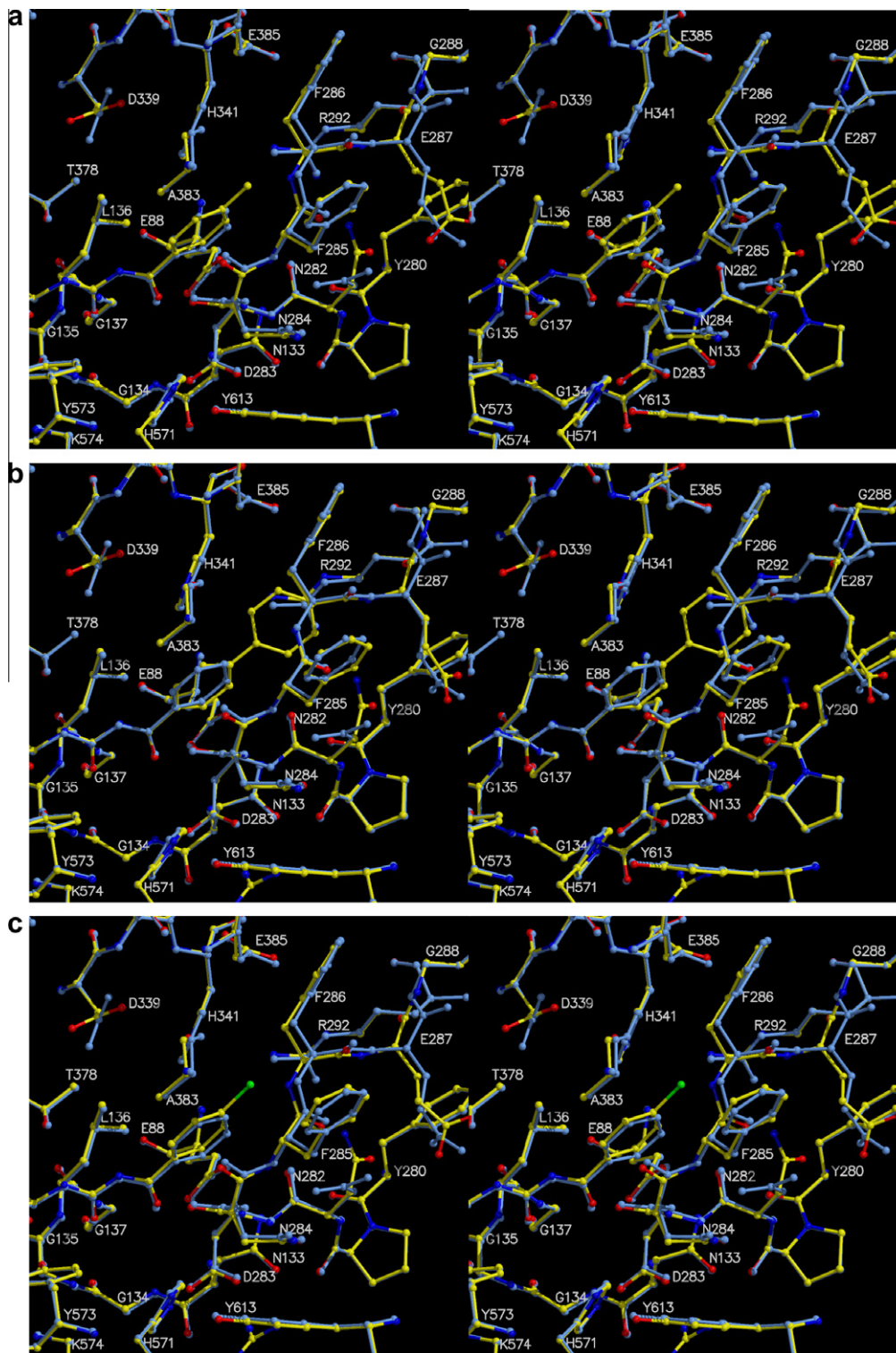


Figure 3. Stereo diagrams of the structures of RMGPb in complex with Bzurea (**15**) (shown in dark; cyan in web) and compounds **25** (a) **26** (b), **27** (c), **28** (d), **29** (e), **30** (f) (shown in light grey; yellow in web).

Wat244 O (by $\sim 0.5\text{\AA}$) and waters Wat86 O, Wat251 O, Wat42 O, Wat224 O and Wat245 by $\sim 0.4\text{\AA}$. Although the perturbation that compound **30** induced is rather limited analogous to the one of **28** the structural results suggest that possibly the cost of the conformational energy to transfer the compound from the solvent to the catalytic site of the RMGPb could not be compensated by the increased hydrogen bond interactions formed.

2.3. Computational studies

Recently, computational studies on small molecule inhibitors of glycogen phosphorylase were surveyed.²² Also, the performance of different docking programs were evaluated on glycogen phosphorylase.²³ This study showed that the **GLIDE** docking program was the best performing one with the lowest RMSD to the crystal structure

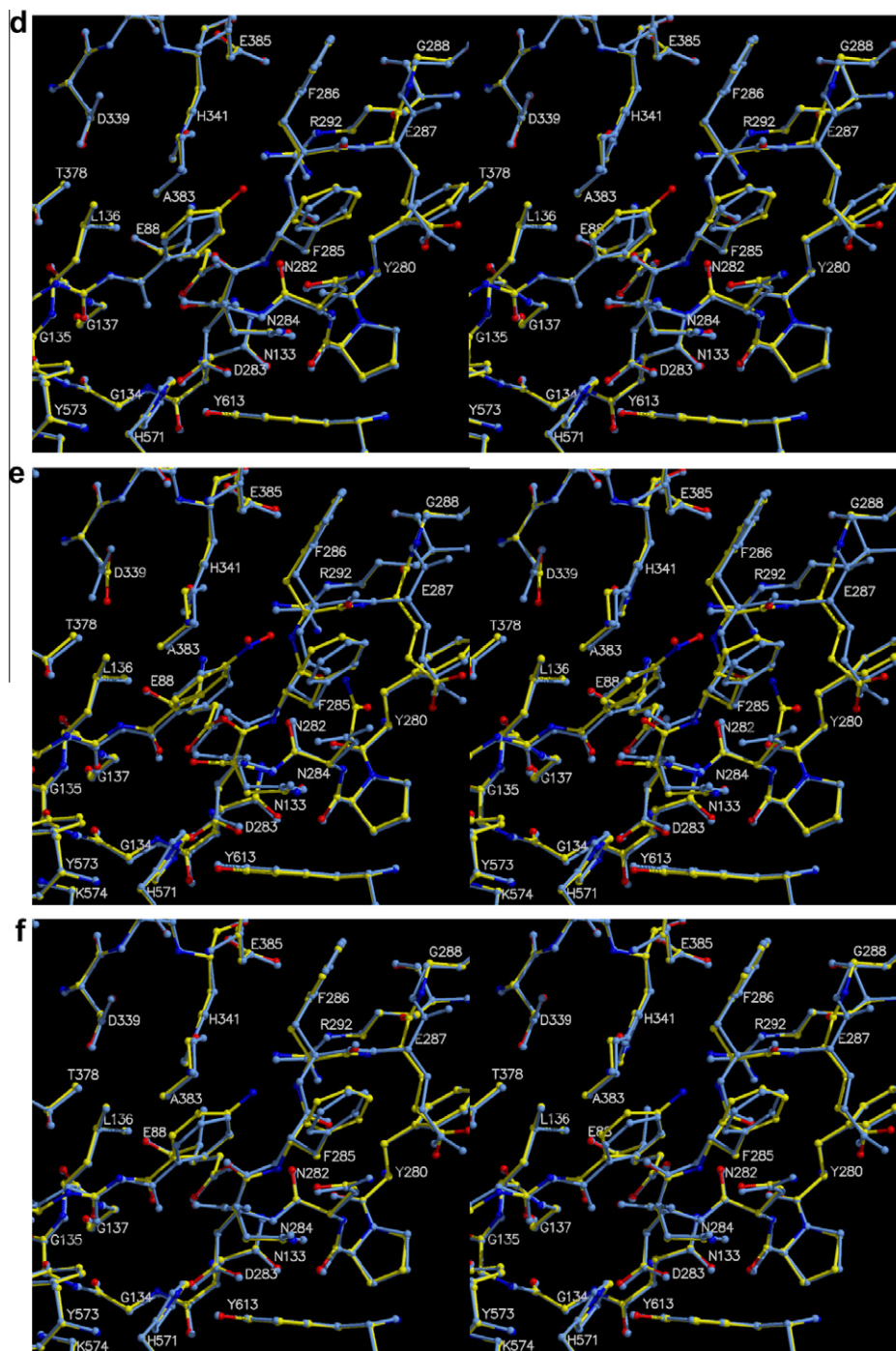


Fig. 3 (continued)

orientations and that scoring function in the **GLIDE** program correlate well with experimental K_i values.²⁴

In the present study, to further test the predictive power and reliability of available computational methods, nine inhibitors were docked to two glycogen phosphorylase structures derived from complexes of RMGPb with inhibitors **15** (protein structure called Bzurea) and *N*-(2-naphthoyl)-*N'*-(β -D-glucopyranosyl)urea (Fig. 4) (protein structure called 2-Nap-urea) using the **GLIDE** program. The docked inhibitors conformations with the lowest GlideScore were chosen for further evaluation of binding affinity using LiaScore calculated with **LIAISON** program. The resulting scores are compared with experimental K_i , computed $\ln K_i$ and ΔG values in

Table 2. The comparison of the geometry of docked structure for inhibitor **15**-Bzurea and *N*-(2-naphthoyl)-*N'*-(β -D-glucopyranosyl)urea-2-Nap-urea complexes can be seen in Figures 5 and 6, respectively. Figure 7 shows the best docked poses for all inhibitors in the active site of 2-Nap-urea glycogen phosphorylase. Correlation of experimental $\ln K_i$ values with predicted LiaScore is given in Figure 8.

To evaluate the accuracy of Glide docking, the best docked poses of **15** and 2-Nap-urea were compared with their X-ray conformations in complex with the glycogen phosphorylase and **pyridoxal-5'-phosphate**. The best poses for the docked structures were chosen on the bases of the GlideScore. First, we noticed that the docked

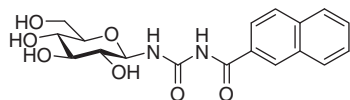


Figure 4. Structure of inhibitor *N*-(2-naphthoyl)-*N'*-(β-D-glucopyranosyl)urea (K_i 0.35 μM).¹⁷

poses were correctly predicted (Figs. 5 and 6). It appears that a better accuracy was observed for the case of the 2-Nap-urea complex. This is also documented by the calculated RMSDs of 2.117 Å for Bzurea and 0.726 Å for 2-Nap-urea complex, respectively. Second, a thorough analysis of the docked structure in Bzurea indicates that glucose location is correctly predicted and the main deviation comes from the urea part. The glucose moiety of **15** makes H-bond interactions with protein side chains, namely Glu672 and Asn484, similarly as in the crystal structure, however due to different orientation of the C6 hydroxyl group, does not interact with His377. The urea conformation presented in the docked pose is *s*-trans whereas in the crystal structure is *s*-cis. This conformational change is responsible for slightly different binding of the phenyl group. We assume that a removal of water molecules from protein structure might be one of the reasons for the conformational change. In fact, the interactions of these water molecules with the urea carbonyls in crystal structure are not assumed in docking procedure. We note that the phenyl moiety is partially exposed to solvent and the phenyl ring interactions might not be well described in the scoring function. It is noteworthy that docking of **15** into the binding site of 2-Nap-urea led to the docked pose with the *s*-cis conformation of urea part as it is in crystal structure of Bzurea (not shown). Figure 7 shows that the binding mode of all studied inhibitors is similar to that of **15**. Also the relevant glucose-protein interactions observed in **15** complex are preserved. Measured RMSD values (Å) for the best docked poses of the inhibitors are shown in the Table 2. RMSD was measured only between heavy atoms in the common inhibitors parts, namely *N*-benzoyl-*N'*-(β-D-glucopyranosyl) urea part. Values for RMSD are in interval 1.009–6.858 Å for Bzurea and 0.680–2.382 Å for 2-Nap-urea structures, respectively. These values indicate that structures docked into the 2-Nap-urea structure are more precise as documented by smaller RMSD values. The largest observed RMSD of 6.858 Å is for the **29** docked pose in the Bzurea structure. On the other hand, **29** has the lowest measured RMSD value 0.680 Å in the 2-Nap-urea structure. The smaller RMSD of 1.009 Å in the Bzurea is found for **30**. The largest difference from the 2-Nap-urea X-ray structure was observed for **15**. This might reflect an influence of the larger binding pocket, which has responsibility for a different binding mode.

It is well known that the docking accuracy of ligand depends on the protein structure. When docking **15** into the Bzurea and

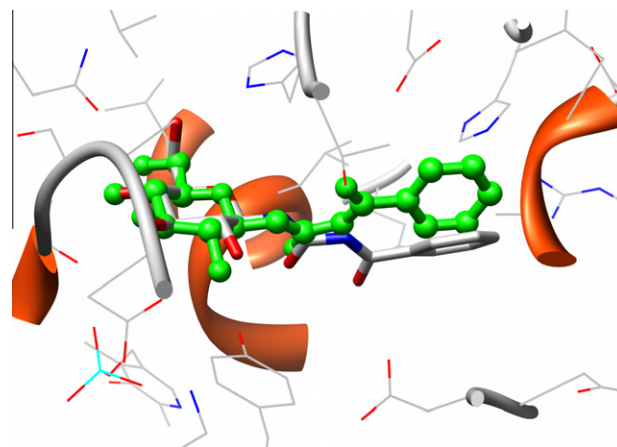


Figure 5. The docked structure of inhibitor **15** into binding site of the glycogen phosphorylase Bzurea structure, crystal structure shown in sticks, docked structure in ball and stick representation. The calculated RMSD is 2.117 Å.

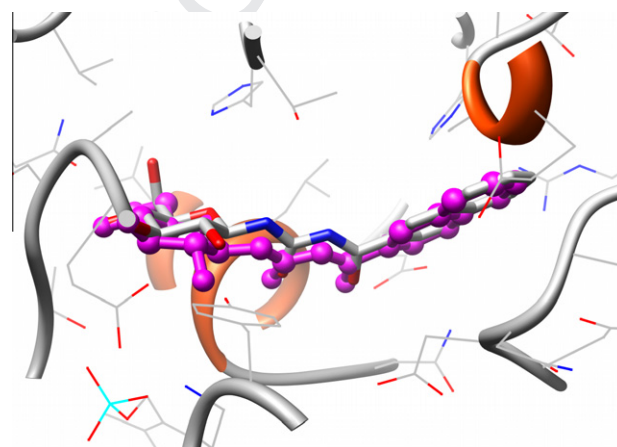


Figure 6. The docked structure of the inhibitor *N*-(2-naphthoyl)-*N'*-(β-D-glucopyranosyl)urea into binding site of the glycogen phosphorylase 2-Nap-urea structure, crystal structure shown in sticks, docked structure in ball and stick representation. The calculated RMSD is 0.726 Å.

2-Nap-urea structures of the glycogen phosphorylase we have also observed small differences, as discussed above. This led us to consider refinement and rescoring of docking poses using LAISON program, in which the flexibility of protein, or more precisely the flexibility of protein side chains, is to some extent taken into account. Therefore, all saved docking poses from Glide docking

Table 2
Comparison of the experimental data with the calculated GlideScores, LiaScores and RMSD to the X-ray ligand common part for the best docked into binding site of Bzurea and 2-Nap-urea structures of glycogen phosphorylase

Name	Experiment			Bzurea			2-Nap-urea		
	K_i (μM)	$\ln K_i^a$ (μM)	ΔG^a (kcal/mol)	Gscore	LiaScore	RMSD	Gscore	LiaScore	RMSD
25	2.3	0.8329	-7.74	-6.99	-12.98	1.626	-7.07	-13.12	2.009
31	3.2	1.1632	-7.55	-6.70	-15.09	1.997	-8.60	-12.49	0.907
29	3.3	1.1939	-7.52	-6.78	-14.25	6.858	-8.70	-15.61	0.680
26	3.7	1.3083	-7.46	-7.80	-14.81	1.732	-8.05	-14.59	1.785
32	4.0	1.3863	-7.41	-7.35	-13.60	3.761	-7.71	-14.26	2.260
27	4.4	1.4816	-7.35	-7.97	-13.11	1.753	-7.52	-13.54	1.987
15	4.6	1.5261	-7.33	-7.38	-11.14	2.117	-7.30	-12.99	2.382
30	6.0	1.7918	-7.17	-7.48	-11.32	1.009	-8.56	-11.97	0.924
28	6.3	1.8405	-7.14	-8.26	-12.55	2.219	-8.28	-10.30	1.334

Experimental K_i values are taken from Table 1.

^a Calculated from K_i values.

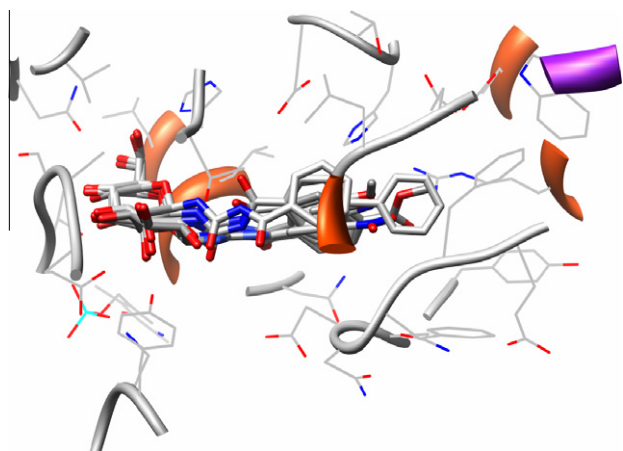


Figure 7. Overlays of the best docked poses of inhibitors into binding site of the glycogen phosphorylase 2-Nap-urea structure. Docked structures are shown in stick representation.

were used as starting position and were fully optimized using Liaison and resulting structures were ranked using LiaScore. The results are listed in Table 2. Then we turned our attention to the comparison of the predicted activities with the experimental data. As can be seen from data in Table 2, the most active **25** was not predicted as the strongest inhibitor of the set with both score functions and for both protein structures. GlideScore for any of the protein structure does not correlate well with the observed activities (R^2 values are around 0.1 with opposite slope and linear correlation was not observed). The Liaison results appeared as the best and LiaScore correlate with experimental data reasonably well. The computed R^2 values for both receptors are given in Table 3. We have performed three different linear fits for both receptors. The first one included all computed LiaScore's. Values of **25** were excluded in the second and values for **25** and **31** in the third linear fit, respectively. The calculated R^2 values are in the interval from 0.3137 to 0.6455 and from 0.3067 to 0.9501 for Bzurea and 2-Nap-urea protein structure, respectively. Calculated R^2 values show that for all data and **25** excluded fits the results are comparable. For 2-Nap-urea structure fit, an improvement was found after the exclusion of both outliers **25** and **31**. However, for Bzurea structure fit the worse R^2 value was observed (Table 3). However, the best

Table 3

Comparison of the R-squared (R^2) for the LiaScore versus $\ln K_i$ fit for both receptors with different data sets

	Bzurea	2-Nap-urea
All data fit	0.31373	0.30675
data w/o 25 fit	0.64555	0.57601
data w/o 25 and 31 fit	0.55054	0.95005

prediction strength we observed with fit without both outliers **25** and **31**, which correctly predict affinity order of the docked structures except for both outliers, of course. For the third fit, in which the inhibitors with the largest difference (**25** and **31**) were excluded, the calculated R^2 value is 0.9501. Different results of docking using Bzurea and 2-Nap-urea protein structures show an important role of the used protein structure on the prediction of inhibitors potency, though these data were obtained only with nine ligands. The protein structure 2-Nap-urea was found to be a fair representative of protein structure for virtual screening. We assume that larger binding site of 2-Nap-urea compared to that in Bzurea is responsible for this fact. On all data we applied linear regression, with general equation $\text{LiaScore} = A + B \cdot \ln K_i$, where A and B are regression parameters. As expected, the best correlation was found for LiaScore with 2-Nap-urea protein structure. The results are plotted on Figure 8 together with 95% confidence limit. The resulting regression parameters are -24.15 and 7.20 with error 1.12 and 0.74, respectively, and the value of R^2 is 0.9501. The correlation between calculated LiaScore and experimentally measured K_i values is good. On Figure 8 can be seen that except value for two outliers, **25** and **31**, all predicted values are in the range of 95% confidence limits. The largest deviation from the correlation, as expected, was observed for **25**. The experimental value of K_i for the **25** is 2.3 μM whereas predicted K_i applying correlation equation from the Liaison is 4.6 μM . The second largest difference has been observed for the **31**. The experimental K_i value is 3.2 μM in this case, the predicted K_i value from the regression equation is 5.0 μM . The second correlation where only **25** was excluded from the fit ($R^2 = 0.5760$), has A and B values -20.53 and 5.00 with an error of 2.59 and 1.75 respectively. The predicted K_i values with this correlation for **25** and **31** are 4.4 and 5.0 μM , respectively. The difference between these two correlations is negligible. The comparison of predicted and experimental K_i values for **25** and **31** shows that predicted K_i value for **25** and **31** are underestimated. At present,

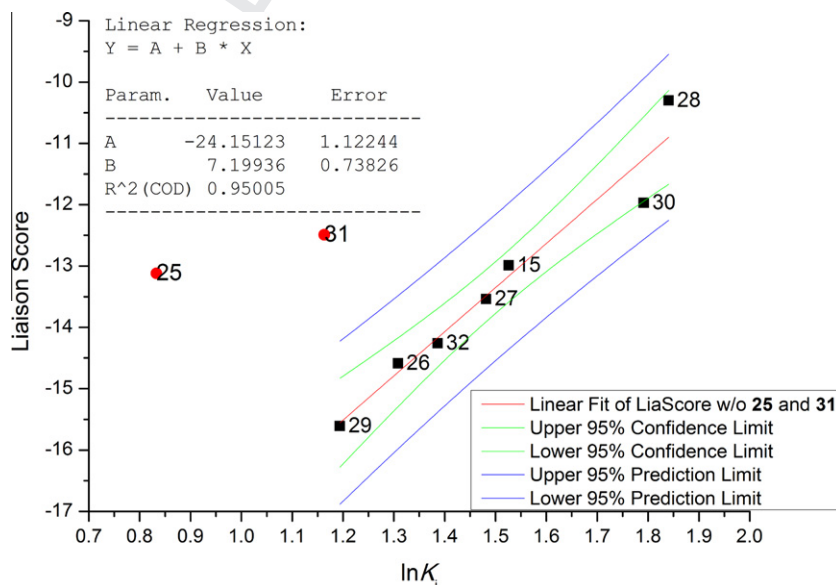


Figure 8. Plot of correlation of experimental $\ln K_i$ values with predicted LiaScores for the docked poses in 2-Nap-urea structure. The compounds **25** and **31** were excluded from the fit.

we have no rational for such a large error. However, we cannot exclude a possibility of a different binding mode for these inhibitors, caused by the so called 280s loop (280–289 amino acid residues) flexibility. Also it is known that lipophilic and stacking interactions of the methylphenyl group are usually poorly described by scoring functions. We also note that our case is not unique, e. g. swainsonine that is most active inhibitor of mannosidase II was predicted to be one of the weakest inhibitors with several scoring functions, though its binding mode was predicted correctly. This shows that there is a room for improvement of scoring functions.

3. Conclusions

N-(4-Substituted-benzoyl)-*N'*-β-D-glucopyranosyl urea derivatives were prepared by ZnCl₂ catalysed acylation of *O*-peracetylated β-D-glucopyranosyl urea or reacting *O*-peracetylated β-D-glucopyranosylamine with acyl-isocyanates and subsequent deprotection. Some compounds were prepared, to avoid protecting group manipulations, in reactions of β-D-glucopyranosylammonium carbamate with acyl-isocyanates. Substituents of neutral polar and apolar as well as acidic and basic character were introduced in the 4-position of the phenyl ring with the aim to exploit the available space at the subsite of the β-pocket of the active site of glycogen phosphorylase taking into account the solvent structure. Most of the new compounds were low micromolar inhibitors of rabbit muscle glycogen phosphorylase b, however, no significant improvement of the inhibitory efficiency as compared to that of *N*-benzoyl-*N'*-β-D-glucopyranosyl urea could be observed. These findings might indicate the lack of a specific and crucial interaction from this position within the catalytic site.

Crystallographic analyses of the 3D structures of the new compounds with RMGPb showed clearly that all analogues induced a more extended shift of the backbone atoms of the 280s loop compared to RMGPb:15. This shift was facilitated by the flipping of the peptide bond formed between Glu287 and Gly288 to create more space at the catalytic site of the enzyme. The most profound differences were observed in the side chain of Asn282 that adopted a modified conformation upon ligand binding in all complexes except for –OH and –NH₂ groups. Overall, the structural results were in accordance with those obtained by the kinetic evaluation of the compounds. The best inhibitor identified was compound 25 (4-CH₃ group) that formed increased van der Waals interactions with the residues lining the catalytic site. The second best inhibitor, out of those studied by X-ray crystallography, was compound 29 (4-NO₂ group) that stabilized the closed conformation of the 280s loop and as well as residues at the far end of the β-pocket such Arg292 through an extended network of water-mediated interactions. Compound 29 formed the largest number of hydrogen bonds at the catalytic site compared to the rest of the compounds. The results obtained suggest the key role of the solvent structure in structure-based ligand design. This could be exploited for the design of more potent inhibitors of enzyme activity coupling the knowledge derived from each complex structure with geometric algorithms.²⁵

The compounds 15, 25–32 were docked into the Bzurea and 2-Nap-urea crystal structure of the glycogen phosphorylase, respectively. The binding affinity of the highest ranked docked poses was predicted by the LIAISON program (LiaScore) and correlated with experimentally measured *K_i* values of the studied inhibitors. The quality of the correlation was assessed using the R-squared (*R*²) coefficient. The value of the *R*² ranges from 0.1080 up to 0.9180. Generally, a better correlation was found for the structures docked into the 2-Nap-urea structure. The best correlation was achieved for the correlation where two outliers, 25 and 32, were excluded from the linear fit, with linear correlation coef-

ficients A and B ($A + B * x$) having values of -23.89 and 7.12. Interestingly, the best measured inhibitor appears as an outlier. This situation might be caused by the different binding mode predicted by the docking and absence of the water molecules present in the active site as have been shown in presented crystal structure. Despite all this, presented linear fit can be used to predict the binding affinity for compounds having the same scaffold structure by the LIAISON program.

4. Experimental

4.1. General synthetic methods

Melting points were measured in open capillary tubes or on a Kofler hot-stage and are uncorrected. Optical rotations were determined with a Perkin-Elmer 241 polarimeter at room temperature. NMR spectra were recorded with Bruker WP 200 SY (200/50 MHz for ¹H/¹³C), Bruker AM 360 (360/90 MHz for ¹H/¹³C) or Bruker AM 400 (400/100 MHz for ¹H/¹³C) spectrometers. Chemical shifts are referenced to Me₄Si (¹H), or to the residual solvent signals (¹³C). TLC was performed on DC-Alurolle Kieselgel 60 F₂₅₄ (Merck) (eluent EtOAc–hexane 1:2, unless stated otherwise), and the spots were visualized under UV light and by gentle heating. For column chromatography Kieselgel 60 (Merck, particle size 0.063–0.200 mm) was used. Organic solutions were dried over anhydrous MgSO₄ and concentrated under diminished pressure at 40–50 °C (bath temperature). Acetonitrile was distilled from P₄O₁₀ and stored over molecular sieves (3 Å). Dry methanol was distilled from magnesium methylate. Other solvents of commercial analytical grade quality were used without further purification.

4.2. General methods for the preparation of *N*-acyl-*N'*-(2,3,4,6-tetra-*O*-acetyl-β-D-glucopyranosyl)ureas

4.2.1. Method A

To a solution of an acyl chloride (7.7 mmol) in 20 ml of dry chloroform anhydrous zinc chloride (80 mg, 0.59 mmol) and 2,3,4,6-tetra-*O*-acetyl-β-D-glucopyranosyl urea (16, 1 g, 2.56 mmol) were added with stirring. The reaction mixture was refluxed until TLC showed the complete transformation of 16. Then the reaction mixture was poured into ice-water and was extracted with chloroform (2×). The organic phases were collected and washed with satd aq Na₂CO₃ solution and water. After drying the solvent was evaporated and the residue was purified by column chromatography (eluent: EtOAc–hexane = 1:2).

4.2.2. Method B

To a suspension of NaOCN (1.21 g, 18.7 mmol) in dry acetonitrile an acyl chloride (14.4 mmol) in acetonitrile (30 ml) and SnCl₄ (84 μl, 0.72 mmol) were added under argon with stirring. The mixture was stirred under reflux for 8 h and after cooling to rt 2,3,4,6-tetra-*O*-acetyl-β-D-glucopyranosyl amine (18, 1 g, 2.88 mmol) was added under argon. After stirring for 30 min some drops of water were added and the mixture was filtered. The solvent was evaporated and the residue purified by column chromatography (eluent: EtOAc–hexane = 1:1).

4.3. General methods for the preparation of *N*-acyl-*N'*-(β-D-glucopyranosyl)ureas

4.3.1. Method C

A solution of an *N*-acyl-*N'*-(2,3,4,6-tetra-*O*-acetyl-β-D-glucopyranosyl)urea in dry methanol was treated with a catalytic amount

of a methanolic solution of NaOMe at rt. After TLC had shown disappearance of the starting material the reaction mixture was neutralized with a cation exchange resin (Amberlyst 15, H⁺ form). After filtration the solvent was removed and the residue was purified by crystallisation.

4.3.2. Method D

A solution of an *N*-acyl-*N'*-(2,3,4,6-tetra-*O*-acetyl- β -D-glucopyranosyl)urea in dry methanol was treated with a catalytic amount of acetyl chloride at rt. After TLC had shown disappearance of the starting material the reaction mixture was neutralized with solid NaHCO₃. After filtration the solvent was removed and the residue was purified by column chromatography (eluent: CHCl₃–MeOH = 9:1).

4.3.3. Method E

Oxalylchloride (1.1 equiv) was added to a suspension of a carboxamide (0.15 mmol) in anhydrous 1,2-dichloroethane (2 mL) and the mixture was heated at reflux temp. for 1 d. The volatiles were distilled off under diminished pressure and toluene (2 × 5 mL) was evaporated from the residue to remove the rest of oxalylchloride. The acyl-isocyanate obtained in this way was mixed with a solution of β -D-glucopyranosylammonium-carbamate²⁰ (1 equiv) in anhydrous pyridine (100 mg/14 mL) and the mixture was stirred until TLC (CHCl₃–MeOH = 7:1) showed no more change (transformations were incomplete). Pyridine was distilled off under diminished pressure and evaporation of toluene (2 × 30 mL) removed traces of pyridine. The crude was purified by column chromatography (CHCl₃–MeOH = 7:1).

Particular syntheses and compound characterization data are presented in the Supplementary data.

4.4. Enzyme preparation

RMGPb was isolated from rabbit skeletal muscle and purified as described previously.²⁶ Kinetic studies were performed in the direction of glycogen synthesis in the presence of various concentrations of inhibitors as indicated in Table 1. Enzyme activity was measured at pH 6.8 by the release of inorganic phosphate as described previously by Oikonomakos et al.²⁷ (compounds 27, 29 and 30) and Saheki et al.²⁸ (compounds 21, 23 and 25).

4.5. Crystal complex formation and X-ray crystallographic data collection and processing

Native T-state GPb crystals were grown in the tetragonal lattice, space group *P*4₃2₁2²⁹ and prior to data collection were soaked in a buffered solution (10 mM Bes, pH 6.7) with 6.2 mM of 21 (for 2 h), 0.76 mM of 23 (in 20% DMSO for 84 h), 1 mM of 25 (in 2% DMSO for 10 h), 10 mM of 29 (for 1 h). Co-crystals of RMGPb complexed with 27 and 30 were obtained in a medium consisting of 20 mg/ml enzyme, 1 mM spermine, 3 mM DTT, 10 mM BES, 0.1 mM EDTA, 0.02% sodium azide, pH 6.7 (16 °C) with either 5 mM of 27 or 7 mM of 30. Diffraction data for all complexes were collected from single crystals at room temperature, using synchrotron radiation source at EMBL-Hamburg outstation, Germany, beamlines X31 (λ = 0.8123 Å), X11 (λ = 0.813 or 0.8468 Å), BW7A (λ = 0.9076 Å) and BW7B (λ = 0.8441 Å), and SRS-Daresbury Laboratory, beamline PX9.6 (λ = 0.92 Å). Integration of the reflections and data reduction was performed using the programs DENZO and SCALEPACK from HKL-package.³⁰

4.6. Crystal structure determination

The structure of RMGPb in complex with 15, previously determined at 1.8 Å resolution¹⁶ with XPLOR (pdb code 1K06) was

refined using REFMAC.³¹ The results showed that residues lining the 280s loop exhibited differences in their side chain orientations with the most profound ones localized in residues Asp283 (φ , ψ , χ_1 , χ_2 change by 14°, 51°, 166°, 20°, respectively) and Glu287 (φ , ψ , χ_3 change by 22°, 35°, 156°, respectively). The new model deposited with the protein data bank (pdb code 2QNB), as replacement of 1K06, was used as a starting model for the structure determination of all six complexes. Crystallographic refinement was carried out using a standard protocol as implemented by REFMAC.³¹ 2F_o – F_c and F_o – F_c electron density maps calculated were visualized using the program for molecular graphics 'O'.³² Ligand models were fitted to the electron density maps after adjustment of their torsion angles. Alternate cycles of manual rebuilding with 'O' and refinement with REFMAC improved the quality of the models. The data collection and refinement statistics along with the model quality are summarized in Supplementary data Table S2a.

The stereochemistry of the protein residues was validated by PROCHECK.³³ The analyses of the complex structures comprised mapping of the hydrogen bond and van der Waals interactions of the analogues with the residues lining the catalytic site using CONTACT³³ applying a distance cut off 3.3 and 4.0 Å between the electronegative atoms, respectively. The program calculates the angle O···H···N (where the hydrogen position is unambiguous) and the angle source···oxygen-bonded carbon atom. Suitable values are 120° and 90°. The network of interactions is described in Tables S2b and S2c. Structural comparisons were performed with the program 'O'³² by superposition of the atomic coordinates of the new complexes with those of the RMGPb:Bzurea structure. The root mean square deviation in C α positions were determined for residues (24–249), (261–281), (289–313), (326–549) and (558–830) using LSQKAB.³³

All figures were prepared with the programs MolScript³⁴ and BobScript³⁵ and rendered with Raster3D.³⁶

The coordinates of the new structures have been deposited with the RCSB Protein Data Bank (<http://www.rcsb.org/pdb>) with codes: 2QNB-15, 2QLM-25, 2QLN-26, 2QN3-27, 2QN7-28, 2QN8-29 and 2QN9-30.

4.7. Preparation of protein and ligand structures for docking

The initial structures of the glycogen phosphorylase in a complex with pyridoxal-5'-phosphate and *N*-benzoyl-*N'*- β -D-glucopyranosyl urea 15 and *N*-(2-naphthoyl)-*N'*- β -D-glucopyranosyl urea (2-Nap-urea) were obtained from the PDB database under the codes Bzurea and 2-Nap-urea, respectively, and prepared using Schrodinger's Maestro and Protein Preparation Wizard³⁷ as follows. Water molecules were removed, hydrogen atoms were added and protonation states were assigned based on a residue pK_a's at their normal pH (7.0). Atom types and partial charges were assigned according to the OPLS_2001 force field, also known as OPLS-AA.³⁸

Docking grids were prepared for each of the prepared protein structures, Bzurea and 2-Nap-urea, using the same procedure. The centers of the cubic grid boxes were placed on the centroid of the bound ligands and the box sizes were set to 14 Å in all three dimensions.

Nine inhibitors with available experimental K_i data were selected for this study. The structures of all inhibitors were obtained through the energy minimization using Jaguar v7.0 program included in the Schrodinger software³⁷ at the DFT B3LYP^{39,40} level with the 6-31+G* basis set^{41–46} prior to the docking. The calculated ESP charges were used as input partial charges for ligand atoms in the docking calculations.

Docking was carried out using the Glide v4.5 package of Schrodinger suite 2007.³⁷ Recent review of docking programs showed⁴⁷ that Glide belongs amongst the most accurate docking programs.

We have used flexible ligand docking with the standard precision (SP) algorithm.⁴⁸ The parameters for van der Waals radii were scaled by 0.80 for ligand atoms with partial atomic charge less than 0.15. Ligand poses were clustered with RMSDs less than 0.5 Å and within maximum atomic displacement less than 1.3 Å. After the docking procedure 20 poses of each docked ligand with the best GlideScore⁴⁹ were saved and used for the analysis.

Binding affinities were recalculated for all saved docking poses employing the program Liaison included in the Schrodinger software.³⁷ The structures of the complexes using the OPLS2005 force field⁵⁰ were optimized and the LiaScore's ('GlideScore in Liaison') analyzed for the relaxed complexes. Enzyme ligand complexes were optimized with a restrained mobility of receptor residues at distance larger than 12 Å and with frozen residues at distance larger than 16 Å from ligand, respectively. The same DFT calculated partial atomic charges were used for the ligand as for the docking. Implicit solvent continuum model have been used in computation to model solvent effects. The calculated LiaScore for the best docked pose were correlated with the experimentally measured $\ln K_i$ values.

Acknowledgments

This work was supported by the Hungarian Scientific Research Fund (OTKA T37210, T46081, CK77712) as well as by the TÁMOP 4.2.1/B-09/1/KONV-2010007 project co-financed by the European Union and the European Social Fund. Financial aid to the collaboration between Athens and Debrecen (GR-4/03) as well as Lyon and Debrecen (F-11/05) was provided by GSRT (Greece) as well as EGIDE (France), respectively, and the Agency for Research Fund Management and Research Exploitation (KPI, Hungary), and also by CNRS (France) and the Hungarian Academy of Sciences (PICS 4576). VN thanks the French Embassy in Budapest for supporting her co-tutored PhD Thesis prepared in Lyon and Debrecen. Additional support for this work was provided by Greek GSRT through ENTER-EP6/2001, PENED-204/2001, the Joint Research and Technology Projects between Greece and Hungary (2005–2007), Marie Curie Host Fellowship for the Transfer of Knowledge (ToK) contact no MTKD-CT-2006-042776 under FP6; the FP7 Capacities coordination and support actions REGPOT-2008-1-No 230146 'EUROSTRUCT' and REGPOT-2009-1-No 245866 'ARCADE'; The research leading to these results has received funding from the European Community's Sixth (RII3/CT/2004/5060008, IHPP HPRI-CT-1999-00012) and Seventh Framework Programme (FP7/2007–2013) under grant agreement No. 226716 awarded to both SRS-Daresbury Laboratory and EMBL-Hamburg outstation. We would also like to thank Agence Nationale de la Recherche for funding ANR-08-BLAN-0305 'GPdia' project coordinated by JPP for supporting our collaborative research network and acknowledge the assistance of the staff at EMBL beamlines X31, X13, BW7A, BW7B, at the DORIS storage ring in Hamburg and at SRS-Daresbury beamline PX9.6 for providing excellent facilities for X-ray data collection.

Supplementary data

Supplementary data (details of syntheses and crystallographic analyses) associated with this article can be found, in the online version, at doi:10.1016/j.bmc.2011.12.059.

References and notes

- Alberti, G.; Zimmet, P.; Shaw, J.; Bloomgarden, Z.; Kaufman, F.; Silink, M. *Diabetes Care* **2004**, *27*, 1798.
- Moller, D. E. *Nature* **2001**, *414*, 821.
- Praly, J. P.; Vidal, S. *Mini-Rev. Med. Chem.* **2010**, *10*, 1102.
- Ross, S. A.; Gulve, E. A.; Wang, M. H. *Chem. Rev.* **2004**, *104*, 1255.
- Gershell, L. *Nat. Rev. Drug Disc.* **2005**, *4*, 367.
- Radziuk, J.; Pye, S. *Diabetes Metab. Res. Rev.* **2001**, *17*, 250.
- Staehr, P.; Hother-Nielsen, O.; Beck-Nielsen, H. *Diabetes Obes. Metab.* **2002**, *4*, 215.
- Kurukulasuriya, R.; Link, J. T.; Madar, D. J.; Pei, Z.; Richards, S. J.; Rohde, J. J.; Souers, A. J.; Szczepankiewicz, B. G. *Curr. Med. Chem.* **2003**, *10*, 123.
- Rotella, D. P. *J. Med. Chem.* **2004**, *47*, 4111.
- Oikonomakos, N. G. *Curr. Protein Pept. Sci.* **2002**, *3*, 561.
- Baker, D. J.; Greenhaff, P. L.; Timmons, J. A. *Expert Opin. Ther. Patents* **2006**, *16*, 459.
- Gimisis, T. *Mini-Rev. Med. Chem.* **2010**, *10*, 1127.
- Loughlin, W. A. *Mini-Rev. Med. Chem.* **2010**, *10*, 1139.
- Chrykina, E. D. *Mini-Rev. Med. Chem.* **2010**, *10*, 1093.
- Somsák, L. *Compt. Rend. Chim.* **2011**, *14*, 211.
- Oikonomakos, N. G.; Kosmopolou, M.; Zographos, S. E.; Leonidas, D. D.; Somsák, L.; Nagy, V.; Praly, J.-P.; Docsa, T.; Tóth, B.; Gergely, P. *Eur. J. Biochem.* **2002**, *269*, 1684.
- Somsák, L.; Czifrák, K.; Tóth, M.; Bokor, É.; Chrykina, E. D.; Alexacou, K. M.; Hayes, J. M.; Tiraidis, C.; Lazoura, E.; Leonidas, D. D.; Zographos, S. E.; Oikonomakos, N. G. *Curr. Med. Chem.* **2008**, *15*, 2933.
- Helferich, B.; Kosche, W. *Chem. Ber.* **1926**, *59*, 69.
- Deng, M. Z.; Caubere, P.; Senet, J. P.; Lecolier, S. *Tetrahedron* **1988**, *44*, 6079.
- Likhoshervostov, L. M.; Novikova, O. S.; Shibaev, V. N. *Dokl. Chem.* **2002**, *383*, 89.
- Gregoriou, M.; Noble, M. E. M.; Watson, K. A.; Garman, E. F.; Krülle, T. M.; Fuente, C.; Fleet, G. W. J.; Oikonomakos, N. G.; Johnson, L. N. *Protein Sci.* **1998**, *7*, 915.
- Hayes, J. M.; Leonidas, D. D. *Mini-Rev. Med. Chem.* **2010**, *10*, 1156.
- Bentlifa, M.; Hayes, J. M.; Vidal, S.; Gueyrard, D.; Goekjian, P. G.; Praly, J.-P.; Kizilis, G.; Tiraidis, C.; Alexacou, K.-M.; Chrykina, E. D.; Zographos, S. E.; Leonidas, D. D.; Archontis, G.; Oikonomakos, N. G. *Bioorg. Med. Chem.* **2009**, *17*, 7368.
- Alexacou, K. M.; Hayes, J. M.; Tiraidis, C.; Zographos, S. E.; Leonidas, D. D.; Chrykina, E. D.; Archontis, G.; Oikonomakos, N. G.; Paul, J. V.; Varghese, B.; Loganathan, D. *Proteins: Struct. Funct. Bioinform.* **2008**, *71*, 1307.
- Chrykina, E. D.; Chajistamatiou, A.; Chegkazi, M. *Curr. Med. Chem.* **2011**, *18*, 2620.
- Melpidou, A. E.; Oikonomakos, N. G. *FEBS Lett.* **1983**, *154*, 105.
- Oikonomakos, N. G.; Kontou, M.; Zographos, S. E.; Watson, K. A.; Johnson, L. N.; Bichard, C. J. F.; Fleet, G. W. J.; Acharya, K. R. *Protein Sci.* **1995**, *4*, 2469.
- Saheki, S.; Takeda, A.; Shimazu, T. *Anal. Biochem.* **1985**, *148*, 277.
- Oikonomakos, N. G.; Melpidou, A. E.; Johnson, L. N. *Biochim. Biophys. Acta* **1985**, *832*, 248.
- Otwinowski, Z.; Minor, W. *Methods Enzymol.* **1997**, *276*, 307.
- Murshudov, G. N.; Vagin, A. A.; Dodson, E. J. *Acta Crystallogr., Sect. D* **1997**, *53*, 240.
- Jones, T. A.; Zou, J. Y.; Cowan, S. W.; Kjeldgaard, M. *Acta Crystallogr., Sect. A* **1991**, *47*, 110.
- Acta Crystallogr., Sect. D* **1994**, *50*, 760.
- Kraulis, P. J. *Appl. Crystallogr.* **1991**, *24*, 946.
- Esnouf, R. M. *J. Mol. Graphics Modell.* **1997**, *15*, 132.
- Merritt, E. A.; Bacon, D. J. *Macromol. Crystallogr., Pt B* **1997**, *277*, 505.
- Schrödinger Suite, 2007. Schrödinger, Inc., Portland, OR.
- Jorgensen, W. L.; Maxwell, D. S.; Tirado-Rives, J. *J. Am. Chem. Soc.* **1996**, *118*, 11225.
- Becke, A. D. *J. Chem. Phys.* **1993**, *98*, 1372.
- Lee, C. T.; Yang, W. T.; Parr, R. G. *Phys. Rev. B* **1988**, *37*, 785.
- Ditchfield, R.; Hehre, W. J.; Pople, J. A. *J. Chem. Phys.* **1971**, *54*, 724.
- Hehre, W. J.; Pople, J. A. *J. Chem. Phys.* **1972**, *56*, 4233.
- Binkley, J. S.; Pople, J. A. *J. Chem. Phys.* **1977**, *66*, 879.
- Hariharan, P. C.; Pople, J. A. *Theor. Chim. Acta* **1973**, *28*, 213.
- Hehre, W. J.; Ditchfield, R.; Pople, J. A. *J. Chem. Phys.* **1972**, *56*, 2257.
- Francl, M. M.; Pietro, W. J.; Hehre, W. J.; Binkley, J. S.; Gordon, M. S.; Defrees, D. J.; Pople, J. A. *J. Chem. Phys.* **1982**, *77*, 3654.
- Englebienne, P.; Fiaux, H.; Kuntz, D. A.; Corbeil, C. R.; Gerber-Lemaire, S.; Rose, D. R.; Moitessier, N. *Proteins: Struct. Funct. Bioinform.* **2007**, *69*, 160.
- Friesner, R. A.; Banks, J. L.; Murphy, R. B.; Halgren, T. A.; Klicic, J. J.; Mainz, D. T.; Repasky, M. P.; Knoll, E. H.; Shelley, M.; Perry, J. K.; Shaw, D. E.; Francis, P.; Shenkin, P. S. *J. Med. Chem.* **2004**, *47*, 1739.
- Eldridge, M. D.; Murray, C. W.; Auton, T. R.; Paolini, G. V.; Mee, R. P. *J. Comput. Aided Mol. Des.* **1997**, *11*, 425.
- Kaminski, G. A.; Friesner, R. A.; Tirado-Rives, J.; Jorgensen, W. L. *J. Phys. Chem. B* **2001**, *105*, 6474.